Published in final edited form as:
Vis Neurosci. 2009 ; 26(4): 365–374. doi:10.1017/S0952523809990162.

The Composition of the Inner Nuclear Layer of the Cat Retina

Margaret A. MacNeil[1,2], **Sheryl Purrier**[1], and **R. Jarrett Rushmore**[3]

[1]Department of Biology, York College of the City University of New York, Jamaica, NY 11451

[2]Department of Biology, CUNY Graduate Center, New York, NY 10016

[3]Laboratory of Cerebral Dynamics, Plasticity and Rehabilitation, Department of Anatomy and Neurobiology, Boston University School of Medicine, Boston, MA 02118

Abstract

The cellular composition of the inner nuclear layer (INL) is largely conserved among mammals. Studies of rabbit, monkey and mouse retinas have shown that bipolar, amacrine, Müller and horizontal cells make up constant fractions of the INL (42%, 35%, 20% and 3%, respectively); these proportions remain relatively constant at all retinal eccentricities. The purpose of our study was to test whether the organization of cat retina is similar to that of other mammalian retinas.

Fixed retinas were embedded in plastic, serially sectioned at a thickness of 1 μm, stained and imaged at high power in the light microscope. Bipolar, amacrine, Müller and horizontal cells were classified and counted according to established morphological criteria. Additional sets of sections were processed for protein kinase C and calretinin immunoreactivity to determine the relative fraction of rod bipolar and AII amacrine cells.

Our results show that the organization of INL in the cat retina contains species specific alterations in the composition of the INL tied to the large fraction of rod photoreceptors. Compared with other mammalian retinas, cat retinas show an expansion of the rod pathway with rod bipolar cells accounting for about 70% of all bipolar cells and AII cells accounting for nearly a quarter of all amacrine cells. Our results suggest that evolutionary pressures in cats over time has refined their retinal organization to suit its ecological niche.

Keywords

rod bipolar cells; AII amacrine cells; horizontal cells; photoreceptors; immunofluorescence

Introduction

The structure of the vertebrate retina is not the same for every species, but is modified according to the visual demands placed on the animal. These changes have been described most extensively at the ganglion cell layer (Stone, 1983; Land & Fernald, 1992). Prey animals, such as the rabbit, have a horizontal strip of elevated ganglion cell density that enables an increased visual sampling at locations most likely to detect predators (Hughes, 1977; Stone, 1983; Ahnelt & Kolb, 2000). Similarly, predators that require high resolution vision typically contain a region of the retina at the center of the optical axis that demonstrates an increased ganglion cell density (area centralis). Fish that view the surface of the water have an increased ganglion

Correspondence: Margaret A. MacNeil, Ph.D., York College, CUNY, Department of Biology, 94-20 Guy R. Brewer Blvd., Jamaica, NY 11451, Phone: 718-262-2711, Fax: 718-262-2369, macneil@york.cuny.edu.

cell density in the inferior retina, while fish that predominantly look beneath them have a corresponding area in the upper retina (Collin & Pettigrew, 1988).

Similar comparative examinations have been done in the photoreceptor layer. Here, too, the distribution and proportion of the two types of photoreceptors inform on the nature of the animal: animals with rod dominated retinas, such as the rat, typically occupy nocturnal environments, whereas diurnal animals, such as the macaque, have retinas with a mixture of rods and cones to register visual stimuli in photopic and scotopic conditions (Linberg *et al.*, 2001).

The composition of the inner nuclear layer (INL), located between the ganglion cell and photoreceptor layers, has not been extensively compared among species, and differences in its structure have not been reported. This layer is made up of three neural cell classes that relay the visual signals from the photoreceptors to the ganglion cells, and sculpt the signals into visual streams (Masland, 2001; Wässle, 2004). In mice, macaques and rabbits, bipolar cells make up about 40% of the cells, horizontal cells are 2%, and amacrine cells comprise 35% (Martin & Grünert, 1992; Strettoi & Masland, 1995; Jeon et al., 1998). The retinal support cells, the Müller cells, make up the balance. Comparisons of the cells in the inner nuclear layer of the macaque, the rabbit and the mouse have suggested that the proportion of cells in the inner nuclear layer do not differ significantly among mammals (Jeon et al., 1998). We investigated this question by studying the retina of the cat. We have found evidence that the transretinal rod pathway is expanded and overrepresented in the cat retina relative to species previously investigated.

Materials and methods

The tissue was obtained from four adult cats (Liberty Laboratories, Waverly NY or Harlan, Indianapolis, IA) that had been used for behavioral testing at Boston University. At the completion of those experiments, cats were anesthetized with a large dose of sodium pentobarbital (≥ 65 mg/kg, i.v.) and perfused through the heart with saline followed by 2.5% glutaraldehyde, 2% paraformaldehyde in 0.1M phosphate buffer, pH 7.4. The eyes were extracted from the orbit, the anterior segments removed and the eye cups immersed in the same fixative and stored at 4°C until sectioned. All procedures were approved by the Institutional Animal Care and Use Committee of Boston University School of Medicine and in accord with the Guidelines for the Care and Use of Mammals in Neuroscience and Behavioral Research (National Research Council, 2003).

Tissue Processing

The regions of retina studied included area centralis, and eleven locations in dorsal and ventral retina collected along the vertical meridian. Area centralis was identified in the dissecting microscope by flushing a drop of 1% toluidine blue across temporal retina to lightly stain ganglion cells and view unstained blood vessels that encircled, but did not invade the area. A scalpel was used to excise area centralis from the eyecup and then to extend the incisions dorsally and ventrally to make a vertical strip ~5 mm in width. The excised retina was further divided into 1 mm long segments, 12 in dorsal retina and 10 in ventral retina. The pieces were rinsed in sodium phosphate buffer (3 × 10 min) and post-fixed with 1% osmium tetroxide for 30 minutes. After rinsing, each piece was dehydrated in a graded series of alcohols, embedded in Spurr's resin (Ted Pella, Redding, CA) and incubated in a 70 degree oven for 2–4 days.

After polymerization, 12 blocks from each retina were sectioned to sample the density of cells at multiple retinal eccentricities (Wong & Hughes, 1987). Approximately 50–80, 1 μm thick serial sections from each block were cut using a Leica Ultracut ultramicrotome. Ribbons of sections were mounted onto glass slides and stained with 1% toluidine blue with 1% borax

while heating on a hot plate. The sections were rinsed with dH_2O, dehydrated in 95% ethanol and coverslipped with Permount. Each section was visualized with a Nikon E800 microscope using a 60× Plan Fluor oil immersion objective (NA 1.2) and a 5,400 μm^2 region was imaged from consecutive sections using a Hamatsu Orca cooled ccd camera with MetaVue v6.3 imaging software.

Data Sampling and Analysis

For each eccentricity studied, all INL cells in images from 20 – 30 consecutive sections were identified using standard morphological criteria and counted, a method successfully used by others (McGuire et al., 1984; Strettoi & Masland, 1995). Cells located in this layer included bipolar, amacrine, Müller and horizontal cells and were clearly distinguished from each other by considering the size and shape of the cell bodies, their location within the INL, cytoplasmic staining characteristics and the trajectory of axons and dendrites exiting the cell body (Figure 1). The distinctive morphologies and the relatively large size of cat retinal neurons made it possible to identify every cell in a set of 1 μm thick serial sections using the light microscope. An example of this identification process is demonstrated in Figure 2. Starting with the second image in the series, a cone bipolar cell is visible (asterisk). The cell is elongated with pale staining matrix, and has a stout apical process extending toward the outer plexiform layer (OPL) and a thin distal axon entering the IPL. This identification can be verified by following its processes into adjacent sections. Using the same procedure of following cells through sets of serial sections, all cells in given region can be identified, counted and their relative fractions computed (Strettoi & Masland, 1995).

Immunohistochemistry

To unequivocally identify rod and cone bipolar cells and AII amacrine cells, we stained vibratome sections with antibodies against protein kinase C (PKC; to label rod bipolar cells) or calretinin (to label AII amacrine cells) in a single retina. We did not achieve adequate antibody penetration with wholemount retinas, so we cut sections from five different eccentricities (area centralis (AC), 1, 4, and 8 mm dorsal to area centralis and 4 mm ventral to AC). Small pieces, approximately 2 mm^2, were dissected from the sclera, embedded in agarose (low melting point, Sigma, St. Louis, MO), and sectioned at a thickness of 50 μm using a vibratome. Sections were incubated in 1% sodium borohydride for 30 minutes, rinsed in sodium phosphate buffer (3 × 10 min), and blocked overnight at 4°C in 4% normal donkey serum with 0.5% Triton X-100. The next day, retinas were rinsed in buffer and incubated at 4°C with 2% normal donkey serum, 0.5% Triton-X 100 and mouse anti-PKC (1:200, Upstate, Temecula, CA) or rabbit anti-calretinin (1:200, Swant, Bellinzona, Switzerland). After three days, the retinas were rinsed thoroughly in buffer and incubated for two hours with Alexa Fluor 488 donkey anti-mouse IgG (1:200, Invitrogen, Eugene, OR) or Alexa Fluor 488 donkey anti-rabbit IgG (1:200, Invitrogen, Eugene, OR) and 4 μM ethidium homodimer (Invitrogen, Eugene, OR). After rinsing, sections were mounted onto glass slides, coverslipped in Vectashield (Vector Labs, Burlingame, CA) and imaged at high power in the confocal microscope.

Approximately 20 optical sections, spaced 1 μm apart, were imaged in through focus series in the confocal for each of the five eccentricities studied. At each depth, the tissue was sequentially excited with FITC and Texas Red filters to selectively excite the ethidium homodimer and Alexa Fluor labels. Z-series stacks were opened using Neurolucida (MBL, Williston, VT) and all ethidium-stained nuclei in the INL were identified by scrolling through the stacks of images. The midpoint of each nucleus was determined and that point marked on the image to ensure that the cells in multiple images were counted only once. Using the same procedures, we identified all PKC or calretinin-labeled cells in the same optical sections and computed the fraction of all doubled-labeled cells. The samples comprised at least 400 cells at each of the

five retinal eccentricities. Partially sectioned cells were omitted from the first image of the series and included from the last image of the stack.

Results

Identification of cell classes within the inner nuclear layer

There is a clear difference in the soma sizes and staining patterns of amacrine, bipolar, horizontal, and Müller cells and they were easily differentiated in the prepared tissue. In the INL, amacrine cell somas occupied the innermost layer of cell bodies. Their rounded somas ranged in size from 8 – 12 μm in diameter and all but a thin rim of cytoplasm was occupied by the nucleus, which tended to stain more palely than that of bipolar cells. Often, stout proximal dendrites could be seen extending from the base of the somas to enter the IPL (Figure 3 column A, black arrows); no processes were observed traveling from these cell bodies toward the OPL.

Horizontal cells were the largest cells in the cat retina but were also the least numerous (Figure 3 column B, white arrows). Their large somas had round nuclei with one or two prominent nucleoli and were always positioned close to the OPL. The cytoplasmic matrix was relatively unstained and stout, lateral processes could be followed exclusively into the OPL. No vitreal directed processes were ever observed.

Müller cells had darkly stained matrix and a large amorphous shape that was wedged between amacrine and bipolar cell somas in the middle of the INL. Their processes appeared as thick, dark staining stalks that extended from the cell body to the OPL and to the IPL (Figure 3, column B, black arrows).

Bipolar cells varied most in their location within the INL, staining characteristics of their cell nuclei and matrix, and the size of their somas. The cell somas ranged in size from 6 – 10 μm, with the larger cells tending to have pale matrix as previously described for cone bipolar cells (Cohen & Sterling, 1990) and the smaller, sclerally placed cells stained darkly with ovoid nuclei similar to those found in rod bipolar cells. Nearly all bipolar cell somas occupied the middle of the INL with elongate shapes and processes exiting from both proximal and distal aspects of the cell bodies (Figure 3,column C), although in peripheral retina it was not uncommon to see cone bipolar cells sharing the vitreal layer with amacrine cells (Figure 3C, lower panel). In these instances, cone bipolar cells were distinguished from amacrine cells on the basis of their smaller size, the direction of their processes, and the larger, more prominent nucleoli of the amacrine cells.

In most cases, the largest cells in the INL were found in a single layer located at the boundaries of the INL (amacrine and horizontal cells) with bipolar and Müller cells occupying the middle of the layer. The cells increased in size and the INL decreased in thickness with increasing distance from area centralis.

Distribution of cell classes

After identifying all cells in consecutive semi-thin sections, the numbers of cells within each class were counted at 12 eccentricities in dorsal and ventral retina and the fractions computed (Table 1). In each of the three retinas, the cell densities varied between individuals as well as between retinas of a single animal, but the cells showed similar topographic distributions (Table 1). The highest density of inner nuclear layer cells was located in central retina, just outside area centralis (~112,000 cells/mm^2), reached a plateau in mid-peripheral retina (~80,000 cells/mm^2) and then gradually declined toward the periphery (~50,000 cells/mm^2) (Figure 4A).

Regardless of differences in density between individuals, the relative fractions of the cell classes were remarkably constant, as has been previously shown for rabbit, monkey and mouse retinas (Figure 4). In our tissue, bipolar cells made up the largest fraction of cells in the INL and accounted for 63% of all cells. Amacrine cells and Müller cells accounted for 21% and 15% of cells and horizontal cells were the least numerous cell class and accounted for 1% of the total (Figure 4). Curiously, bipolar cells in the cat retina made up a significantly larger fraction of INL cells than have been observed in other mammals (Strettoi & Masland, 1995;Jeon et al., 1998). In rabbit, mouse and monkey retinas, bipolar cells accounted for 40 – 43% of cells in the INL, compared with 63% that we observed in cat retina. To look more closely at the distribution of bipolar cells in cat retinas, we stained a transect of retina along the vertical meridian with an antibody against PKC and counterstained the retina with ethidium homodimer to label all cells present in the section. Outside central retina, PKC labeled 43% of ethidium homodimer-labeled cells in the INL (Figure 5). Since bipolar cells accounted for 63% of INL cells in the cat retina, we could reasonably estimate that ~ 70% of the total bipolar cell population are rod bipolar cells. This number is significantly larger than the fraction of rod bipolar cells that have been counted in rabbit and monkey retinas, which have been estimated to make up between 8 – 18% of INL cells (Figure 6A) (Martin & Grünert, 1992;Strettoi & Masland, 1995;Jeon et al., 1998). In area centralis, the pattern was somewhat different. Here exists the highest density of cones and the lowest density of rods in the cat retina (Steinberg et al., 1973) and only at this eccentricity did we observe a smaller fraction of rod bipolar cells compared with the numbers of cone bipolar cells (Figure 5). Rod bipolar cells had a density of ~35,000 cells/mm^2 in area centralis compared to a maximum density of ~46,100 cells/mm^2 only 1 mm away. The overall density of bipolar cells did not drop in central retina however, because the decline in rod bipolar cells was offset by an increase in the density of cone bipolar cells, which peaked at 30,200 cells/mm^2.

Since the fraction of rod bipolar cells was considerably greater than that observed in other mammalian species, we wanted to see whether this increase was limited to the rod bipolar cell population or whether there was an expansion of the rod pathway through the INL. Rod bipolar cells do not synapse directly with ganglion cells, but rather indirectly via AII amacrine cells (Kolb & Famiglietti, 1974; Kolb & Nelson, 1983; Strettoi et al., 1992). If rod bipolar cells account for a larger fraction of bipolar cells in cats, one might expect that AII cells would account for a larger fraction of amacrine cells in cat retina compared to other mammals as well. Results from staining a transect of the retina with rabbit anti-calretinin showed that approximately 7% of all cells in the INL stained with rabbit anti-calretinin (Figure 5). The fraction of cells was highest in area centralis (~10%) and then declined to ~6.5% in midperipheral retina and the periphery (Table 1). Since amacrine cells account for only ~21% of all cells in the INL, this would suggest that AII amacrine cells account for approximately one-third of all amacrine cells in the cat retina, a fraction three times larger than in rabbit and mouse retinas (Vaney, 1990; Vaney et al., 1991; Rice & Curran, 2000). In area centralis, AII amacrine cells accounted for 40% of all amacrine cells, approximately 35% of amacrine cells 1 mm away and then 30% at in the midperiphery. In mouse, rabbit and monkey retinas, AII cells account for only 11% of all amacrine cells (Strettoi & Masland, 1996; Mills & Massey, 1999; Rice & Curran, 2000), suggesting that the expansion of the rod pathway in cat retina includes both rod bipolar and AII amacrine cell types.

Discussion

We found that the overall ratio of amacrine cells, Müller cells and horizontal cells in cat retina is nearly identical to what has been observed in the retinas of rabbits, monkeys and mice (Martin & Grünert, 1992; Strettoi & Masland, 1995; Strettoi & Volpini, 2002). However, cats have a disproportionately large fraction of bipolar cells. Bipolar cells significantly outnumbered all other cell classes and accounted for approximately 63% of cells in the INL,

while amacrine cells accounted for only 21% of all cells. This is contrast to other mammals, which show a more even distribution of all cell classes in the INL, suggesting that bipolar cells in the cat retina have undergone morphological specializations that underlie function.

The major discrepancy in the fractions of the cell classes between cats and other mammalian retinas can be explained by the large fraction of rod bipolar cells. Approximately 45% of all cell somas in the cat INL stained for the rod bipolar cell marker, protein kinase C, indicating that 70% of all bipolar cells in cat retinas are rod bipolar cells. This is in contrast to rabbit, mouse and monkey retinas, which have significantly smaller rod bipolar cell populations (8–18%). When the fractions of rod bipolar cells are excluded, the relative distribution of the remaining cell classes in cats are indistinguishable from the distributions of amacrine, Müller, horizontal and cone bipolar cells in other mammalian retinas (Figure 6). These results suggest that retina of the cat contains species specific alterations in the composition of the INL tied to the large fraction of rod photoreceptors.

Comparisons with other studies

In mammals, the rod pathway is made up of three essential cell types: rod photoreceptors, which are highly sensitive to light, a single type of rod bipolar cell that transmits rod signals to the IPL, and the AII amacrine cells that receive inputs from rod bipolar cells on their arboreal dendrites and makes outputs via gap junctions with ON-cone bipolar cell axons and chemical synapses from its lobular appendages onto OFF cone bipolar cell processes (reviewed by Bloomfield & Dacheux, 2001). It would make sense that an expansion of the rod pathway would include changes to each of these cell types. In cat retinas, the distribution profile of rod photoreceptors is inversely related to that of cones. Rod density is lowest in area centralis (200,000 cells/mm^2) where a peak in cone density occurs, rapidly increases to 350,000 cells/mm^2 within 1 mm of area centralis and reaches a peak density of 550,000 cells/mm^2 in the dorsal periphery (Steinberg et al., 1973; Freed et al., 1987; Greferath et al., 1990; Williams et al., 1993). Assuming that the numbers of rod bipolar cells are closely tied to the rod photoreceptor profile, we would expect to see a drop in the fraction of rod bipolar cells within area centralis and a corresponding increase in the cone bipolar cells. This seems to be the case. When we stained a retinal transect with PKC, the fraction of PKC labeled cells was smallest in area centralis (34%) and then increased in the retinal periphery (49%)(Figure 5). Greferath and colleagues observed a similar pattern in the density and distribution of rod bipolar cells after staining cat retinas with PKC. In area centralis, the density of rod bipolars was 42,000 cells/mm^2, increased to 46,000 cells/mm^2 at eccentricities of 1–2 mm from area centralis and then declined to 20,000 cells/mm^2 in the periphery (Greferath et al., 1990). The slight drop in rod bipolar cell density in area centralis can be explained by fewer rods populating central retina (Steinberg et al., 1973; Greferath et al., 1990; Williams et al., 1993), necessitating fewer numbers of rod bipolar cells. The overall fraction of bipolar cells is relatively unchanged because of an increased number of cone bipolar cells that correspond to the increased numbers of cones (Figure 5).

The overall fractions of cells we counted are in close agreement with earlier reports on the composition of the cat retina. In their analysis of the glycinergic pathway, Wässle and colleagues counted cells in horizontal sections of cat retinas and classified them as amacrine, horizontal or bipolar cells by the diameter of their somas and their depth within the INL (Wässle et al., 1986). At the eccentricity studied, about 24% of all neurons were amacrine cells (16,300 cells/mm^2), 75% were bipolar cells (51,400 cells/mm^2) and about 1% were horizontal cells (1050 cell/mm^2), proportions similar to our results. They suggested that at least half of all bipolar cells must be rod bipolar cells if each rod contacts at least one rod bipolar cell and each rod bipolar cell contacted at least 15 rods (Kolb & Nelson, 1983). Freed and colleagues (1987) reached similar conclusions from examining bipolar cell arrays in area centralis. They

estimated that the rod bipolar cell density was ~36,000 cells/mm^2 in area centralis, which is close to our estimate of 35,000 cells/mm^2 (Table 1).

Distribution of AII amacrine cells

Unlike the predictable distributions of the major cell classes in the cat retina, the topographic distribution AII amacrine cells does not match the distribution profile of the rods and rod bipolar cells. Vaney first showed that the density distribution of AII amacrine cells in cat retina is not matched to the topography of the rod photoreceptors (Vaney, 1985). AII cells in whole mounts of fixed retina had a density of 5,300 cells/mm^2 in central retina and declined exponentially toward the retinal periphery (500 cells/mm^2). Our results showed a similar distribution of AII cell densities, although our density estimates were twice the values predicted by Vaney (Figure 5). Some of these differences can be attributed to method; Vaney's counts may have underestimated the true density because of compression of the retina by the coverslip (Vaney, 1985) and our counts were collected from vertical serial sections with the density computed by calculating the fraction of calretinin-stained cells as a fraction of all INL cells. In our tissue, there were also occasional non-AII amacrine cells labeled by calretinin. We did not include these in our counts when the cells were obviously not AII cells (Figure 5B), but it is possible that some of these non-AII cells were inadvertently included, artificially increasing the observed ratio of AII cells in cat retina. This is in contrast to rabbit, mouse and monkey retinas, in which AII cells account for approximately 11% of all amacrine cells regardless of eccentricity (Strettoi & Masland, 1996; Rice & Curran, 2000). This suggests that the fraction of AII cells is higher in central retina, where the density of rod bipolar cells is lowest, helping to reduce convergence of the rod signal and improve the spatial resolution of the rod pathway in central retina.

What is the significance of the expanded rod pathway in cat retinas?

While cats have been described as primarily nocturnal animals (e.g. Ross, 2000; Linberg *et al.*, 2001), there is sufficient evidence to indicate that they occupy both day-time and nighttime environments (Kavanau, 1970, 1971; Kuwabara *et al.*, 1986). Cats also show peaks in activity during the transitions between day and light (a behavioral pattern termed crepuscular (Petter, 1962)), but their activity patterns are not limited to these times. Instead, cats display multiple instances of sleeping and waking episodes during the night and day time (Kavanau, 1971; Kuwabara *et al.*, 1986). This type of dual activity pattern requires versatility in the specializations of the retina that serve to optimize vision in both light and dark domains and it is likely that the composition of the inner nuclear layer in the cat is part of the balance required to be successful in both environments. The cat has both rods and cones, and an expansion of the rod system makes sense when compared to the macaque monkey, and translates to an improved sensitivity of the visual array by reducing the light intensity needed to activate a single dark-adapted rod (Copenhagen et al., 1990).

Unlike the purely crepuscular rabbit, the cat has need of more rods to subserve vision in purely nocturnal environments. As a result, rod photoreceptors in cats are smaller and about five times more numerous than found in rabbits (Hughes, 1977). Even though the convergence ratio of rods to rod bipolar cells is similar in cats and rabbits, the increased numbers of rods in the cat allow for a better developed sensitivity in the dark (Sterling *et al.*, 1988).

It is not immediately clear why the rod system of the cat is expanded relative to that of the mouse. The density of rods in mouse retina is higher than found in other mammals (Steinberg et al., 1973; Greferath et al., 1990; Williams et al., 1993; Jeon et al., 1998). However, the fraction of bipolar cells is not significantly different from rabbits and monkey (Jeon *et al.*, 1998; Strettoi & Volpini, 2002), which suggests that in the mouse, the numbers of rods converging on to rod bipolar cells is significantly greater, thereby limiting their visual acuity.

The increased number of AII amacrine cells in cats would also improve the resolution of the rod pathway by limiting convergence of the existing rod bipolar cells, onto smaller and more numerous AII amacrine cells (Vaney, 1985). Thus, the expansion of rods in the cat may also serve to increase resolution in low-light conditions

The mechanism for generating the increased number of rod bipolar cells and AII amacrine cells in cat retina is not known, although we believe this feature was shaped by evolutionary adaptation. Evolutionary pressures are sufficient to induce these types of rapid changes to anatomical structures. In a study comparing the retina and lateral geniculate nucleus (LGN) of Spanish wildcats and domesticated cats, Williams and colleagues found the brain size of wildcats to be 50% larger than their more derived relations and had 30–35% more retinal ganglion cells and neurons in the LGN (Williams et al., 1993). Even so, the population of rods in the domestic cat retina was at least as great as that observed in the Spanish wildcat and the number of alpha cells was unchanged compared with other ganglion cell types. This suggests that in the domestic cat lineage, genetic and epigenetic mechanisms for maintaining scotopic and motion sensitivity were maintained despite the large decline in LGN size and retinal ganglion cell numbers. Williams suggests that the major mechanism driving these differences may be due to a modulation in the rate of cell death during development. Alternatively, the large numbers of rods could be generated by a protracted period of retinal cell progenitor proliferation, similar to that shown in the retinas of nocturnal owl monkeys (Dyer et al., 2009). In either instance, since the rod bipolar and AII amacrine cells are more recently derived elements of the retina (Nathans, 1999) and likely evolved together, as the numbers of rods increased, it would follow that more rod bipolar and AII amacrine cells would be maintained at constant proportions across the retina to preserve and even improve retinal acuity.

Our results have revealed a substrate for the functional expansion of the scotopic pathway in the cat retina. We have shown that rod bipolar cells and AII amacrine cells represent a larger fraction of cells in the INL that could be useful for improving visual acuity under scotopic conditions. These results argue against a static structure of the INL in all mammals, but rather a flexible plan that takes advantage of organisms' ecological demands.

Acknowledgments

We thank Ms. Claire Folger and Dr. Janet Rollins for help with embedding and serially sectioning the retinas. This work was supported by NIH grants GM 08153 and NS33975 and funding from the PSC-CUNY, #61371-00 39.

Bibliography

Council NR. , editor. Guidelines for the care and use of mammals in neuroscience and behavioral research. Washington, DC: National Academies Press; 2003.

Ahnelt PK, Kolb H. The mammalian photoreceptor mosaic-adaptive design. Progress in Retinal and Eye Research 2000;19:711–777. [PubMed: 11029553]

Bloomfield SA, Dacheux RF. Rod vision: pathways and processing in the mammalian retina. Progress in Retinal and Eye Research 2001;20:351–384. [PubMed: 11286897]

Cohen E, Sterling P. Demonstration of cell types among cone bipolar neurons of cat retina. Philosophical Transactions of the Royal Society of London - Series B: Biological Sciences 1990;330:305–321.

Collin SP, Pettigrew JD. Retinal topography in reef teleosts. II. Some species with prominent horizontal streaks and high-density areae. Brain Behavior and Evolution 1988;31:283–295.

Copenhagen DR, Hemila S, Reuter T. Signal transmission through the dark-adapted retina of the toad (Bufo marinus). Gain, convergence, and signal/noise. Journal of General Physiology 1990;95:717–732. [PubMed: 2110968]

Dyer MA, Martins R, da Silva Filho M, Muniz JA, Silveira LCL, Cepko C, Finlay BL. Developmental sources of conservation and variation in the evolution of the primate eye. Proceedings of the National Academy of Sciences, USA 2009;106:8963–8968.

Freed MA, Smith RG, Sterling P. Rod bipolar array in the cat retina: pattern of input from rods and GABA-accumulating amacrine cells. Journal of Comparative Neurology 1987;266:445–455. [PubMed: 3693619]

Greferath U, Grunert U, Wassle H. Rod bipolar cells in the mammalian retina show protein kinase C-like immunoreactivity. Journal of Comparative Neurology 1990;301:433–442. [PubMed: 2262600]

Hughes, A. The Topography of Vision in Mammals of Contrasting Life Style: Comparative Optics and Retinal Organisation. In: Crescitelli, F., editor. Handbook of Sensory Physiology. Berlin: Springer-Verlag; 1977. p. 615-756.

Jeon CJ, Strettoi E, Masland RH. The major cell populations of the mouse retina. Journal of Neuroscience 1998;18:8936–8946. [PubMed: 9786999]

Kavanau JL. Locomotion and activity phasing of 6 carnivores and a monkey. Experientia 1970;26:1026–1027. [PubMed: 4991271]

Kavanau JL. Locomotion and activity phasing of some medium-sized mammals. Journal of Mammalogy 1971;52:386–403. [PubMed: 4996451]

Kolb H, Famiglietti EV. Rod and cone pathways in the inner plexiform layer of cat retina. Science 1974;186:47–49. [PubMed: 4417736]

Kolb H, Nelson R. Rod pathways in the retina of the cat. Vision Research 1983;23:301–312. [PubMed: 6880030]

Kuwabara N, Seki K, Aoki K. Circadian, sleep and brain temperature rhythms in cats under sustained daily light-dark cycles and constant darkness. Physiology & Behavior 1986;38:283–289. [PubMed: 3797494]

Land MF, Fernald RD. The evolution of eyes. Annual Review of Neuroscience 1992;15:1–29.

Linberg K, Cuenca N, Ahnelt P, Fisher S, Kolb H. Comparative anatomy of major retinal pathways in the eyes of nocturnal and diurnal mammals. Progress in Brain Research 2001;131:27–52. [PubMed: 11420947]

Martin PR, Grünert U. Spatial density and immunoreactivity of bipolar cells in the macaque monkey retina. Journal of Comparative Neurology 1992;323:269–287. [PubMed: 1401260]

Masland RH. The fundamental plan of the retina. Nature Neuroscience 2001;4:877–886.

McGuire BA, Stevens JK, Sterling P. Microcircuitry of bipolar cells in cat retina. Journal of Neuroscience 1984;4:2920–2938. [PubMed: 6502212]

Mills SL, Massey SC. AII amacrine cells limit scotopic acuity in central macaque retina: A confocal analysis of calretinin labeling. Journal of Comparative Neurology 1999;411:19–34. [PubMed: 10404105]

Nathans J. The evolution and physiology of human color vision: insights from molecular genetic studies of visual pigments. Neuron 1999;24:299–312. [PubMed: 10571225]

Petter JJ. Ecological and behavioral studies of Madagascar lemurs in the field. Annals of the New York Academy of Science 1962;102:267–281.

Rice DS, Curran T. Disabled-1 is expressed in type AII amacrine cells in the mouse retina. Journal of Comparative Neurology 2000;424:327–338. [PubMed: 10906706]

Ross CF. Into the light: the origin of Anthropoidea. Annual Review of Anthropology 2000;29:147–194.

Steinberg RH, Reid M, Lacy PL. The distribution of rods and cones in the retina of the cat (Felis domesticus). Journal of Comparative Neurology 1973;148:229–248. [PubMed: 4700509]

Sterling P, Freed MA, Smith RG. Architecture of rod and cone circuits to the on-beta ganglion cell. Journal of Neuroscience 1988;8:623–642. [PubMed: 2828567]

Stone, J. Parallel Processing in the Visual System: The Classification of Retinal Ganglion Cells and Its Impact on the Neurobiology of Vision. New York, London: Plenum Press; 1983.

Strettoi E, Masland RH. The organization of the inner nuclear layer of the rabbit retina. Journal of Neuroscience 1995;15:875–888. [PubMed: 7823187]

Strettoi E, Masland RH. The number of unidentified amacrine cells in the mammalian retina. Proceedings of the National Academy of Sciences, USA 1996;93:14906–14911.

Strettoi E, Raviola E, Dacheux RF. Synaptic connections of the narrow-field, bistratified rod amacrine cell (AII) in the rabbit retina. Journal of Comparative Neurology 1992;325:152–168. [PubMed: 1460111]

Strettoi E, Volpini M. Retinal organization in the bcl-2-overexpressing transgenic mouse. Journal of Comparative Neurology 2002;446:1–10. [PubMed: 11920715]

Vaney DI. The morphology and topographic distribution of AII amacrine cells in the cat retina. Proceedings of the Royal Society London B Biological Science 1985;224:475–488.

Vaney, DI. The mosaic of amacrine cells in the mammalian retina. In: Osborne, NCG., editor. Progress in retinal research. New York: Pergamon; 1990. p. 49-100.

Vaney DI, Gynther IC, Young HM. Rod-signal interneurons in the rabbit retina: 2. AII amacrine cells. Journal of Comparative Neurology 1991;310:154–169. [PubMed: 1955580]

Wässle H. Parallel processing in the mammalian retina. Nature Reviews Neuroscience 2004;5:747–757.

Wässle H, Schafer-Trenkler I, Voigt T. Analysis of a glycinergic inhibitory pathway in the cat retina. Journal of Neuroscience 1986;6:594–604. [PubMed: 3950712]

Williams RW, Cavada C, Reinoso-Suarez F. Rapid evolution of the visual system: a cellular assay of the retina and dorsal lateral geniculate nucleus of the Spanish wildcat and the domestic cat. Journal of Neuroscience 1993;13:208–228. [PubMed: 8423469]

Wong ROL, Hughes A. Developing neuronal populations of the cat retinal ganglion cell layer. Journal of Comparative Neurology 1987;262:473–495. [PubMed: 3667960]

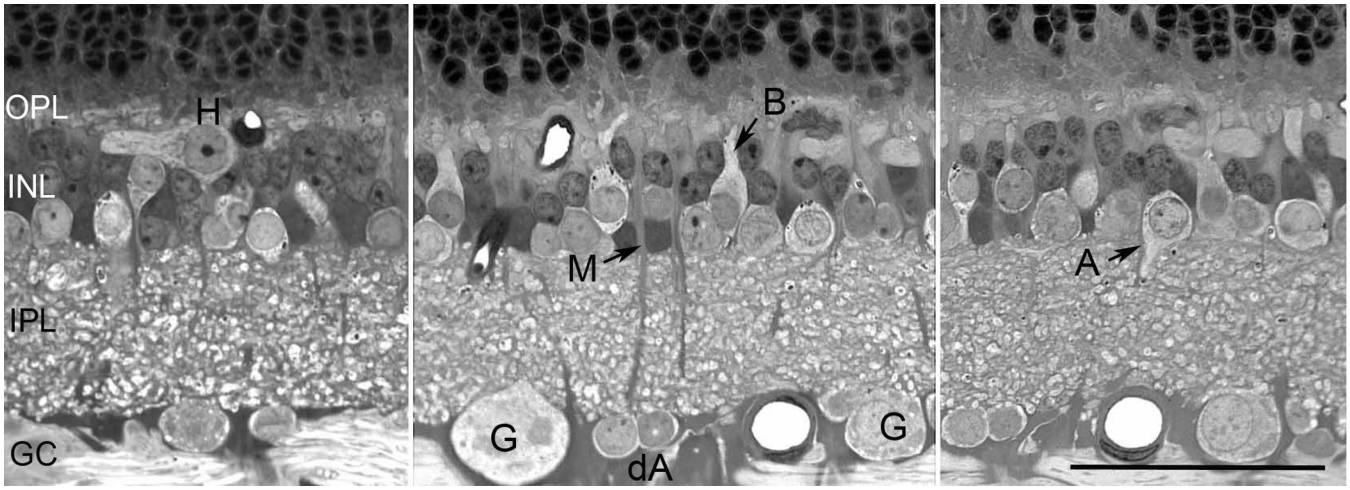

Figure 1.
Vertical sections of the retina to show the characteristics of different cell classes. Cell abbreviations: ganglion (G), displaced amacrine cells (dA), bipolar (B), amacrine (A), Müller (M), and horizontal (H) cells. Scale = 50 μm.

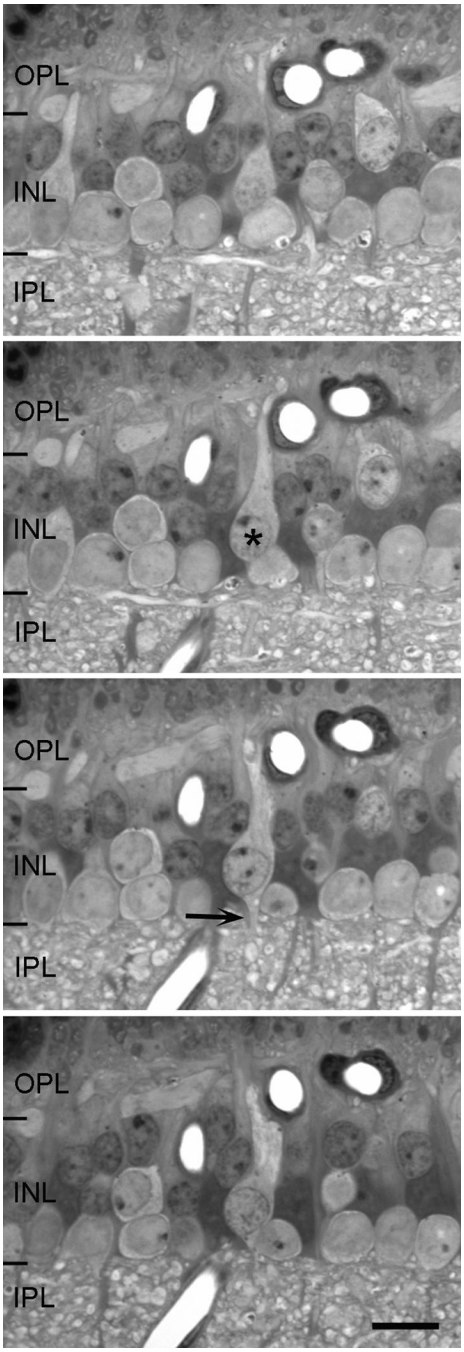

Figure 2.
Four sequential sections, each 1 μm in thickness, of the inner plexiform layer. By looking at consecutive serial sections, it is possible to identify each cell by studying the location of its cell body, its staining characteristics and the termination patterns of its processes. This particular example shows a bipolar cell (asterisk) in vertical section with dendrites reaching toward the outer plexiform layer (OPL) and a thin axon (arrow) exiting from the cell's soma into the inner plexiform layer (IPL). Scale = 10 μm.

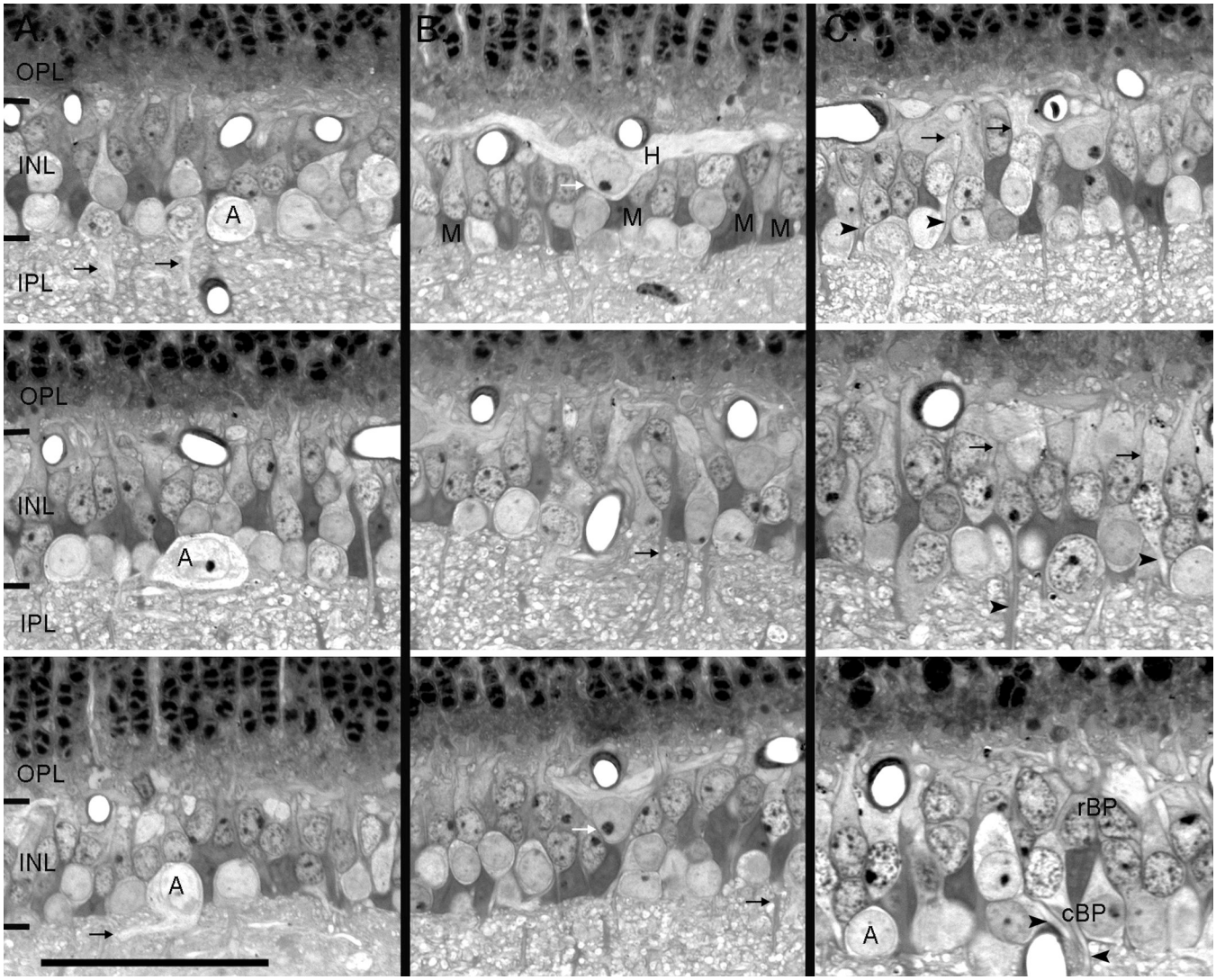

Figure 3.

Vertical sections showing examples of the four cell classes found in the INL. A. Amacrine cells were found in the inner most portion of the INL, were round in shape and had pale staining matrix. They had variously sized cell somas with proximal dendrites (black arrows) that extended into the INL. B. Horizontal cells (white arrows) stained lightly and were found in the outermost layer of the INL and had thick dendritic processes that extended laterally within the OPL. The non-neuronal Müller cells were elongate in shape and had very dark staining somas and stalk like processes that projected into the plexiform layers (black arrows). C. Bipolar cells were elongate in shape and had dendrites that projected toward the OPL (arrows) and thin axons that projected into the IPL (arrowheads). They were most often observed in the middle and outer parts of the INL, but in peripheral retina they intermixed with amacrine cells (lower panel). Cone bipolar cells typically had larger cell somas and paler staining cytoplasm when compared to rod bipolar cells, which were small darkly stained cells that tended to be located in the outer part of the INL. A= amacrine, H = horizontal, M = Müller, rBP = rod bipolar, cBP = cone bipolar. Scale = 25μm.

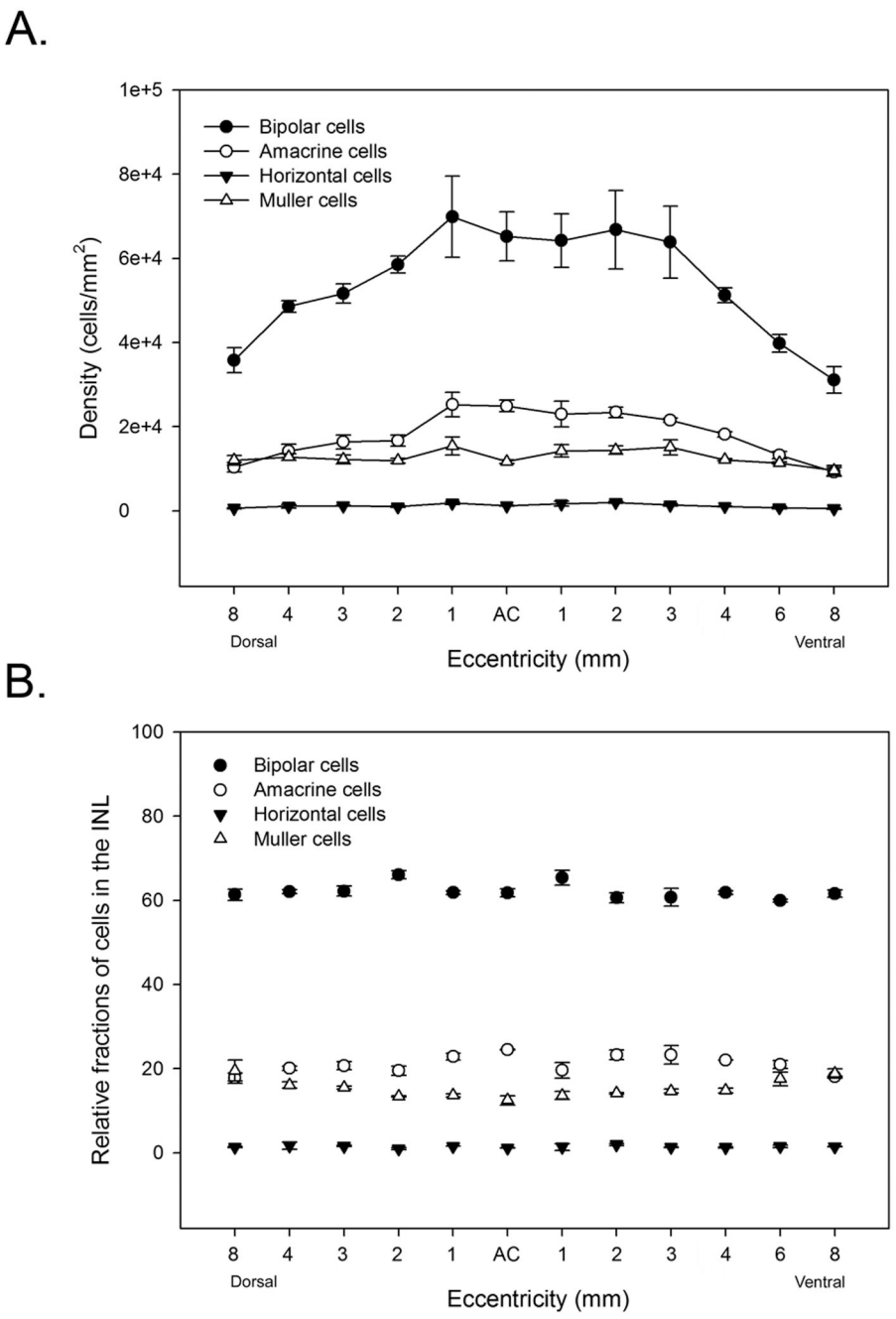

Figure 4.

A. Density of INL cell classes counted from three retinas. Bars represent standard errors. B. Percent of cell classes in the INL of cat retina computed from three retinas with standard errors indicated. Bipolar cells accounted for the largest fraction of cells in the INL of cat retina.

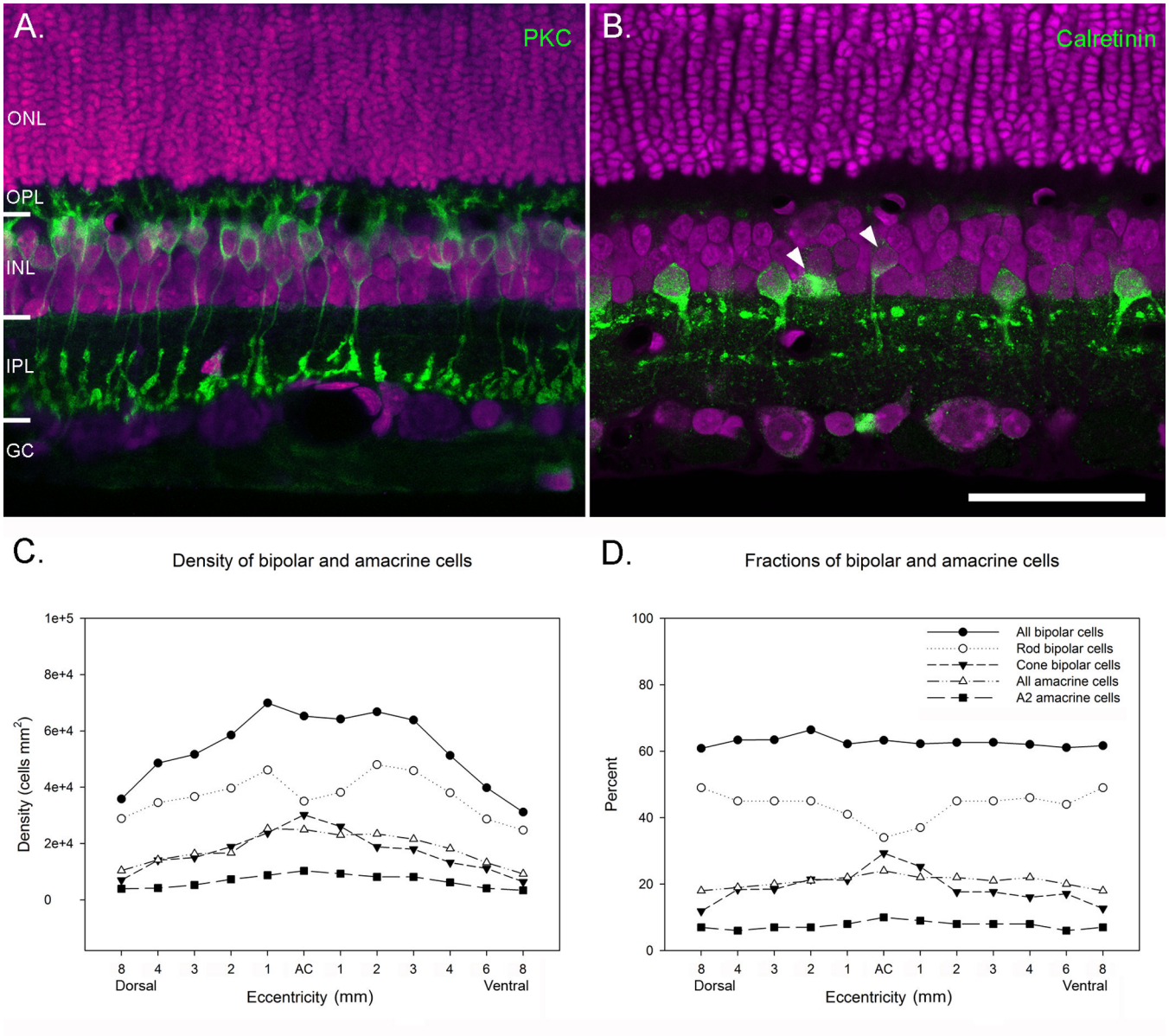

Figure 5.

A. A retinal section stained with an antibody against PKC, to label rod bipolar cells (green) and ethidium homodimer (magenta), to label all cell nuclei. PKC labeled approximately 44% of all cells in the INL. B. A retinal section stained with rabbit anti-calretinin to label AII amacrine cells (green) and ethidium homodimer (magenta). Calretinin stained approximately 7% of all INL cell nuclei. Occasionally, bipolar cells and non-AII amacrine cells were stained also (arrowheads). C. Graph shows the densities of bipolar and amacrine cells across the INL. There was a decline in the numbers of rod bipolar cells in area centralis and a corresponding increase in the numbers of cone bipolar cells. D. Graph shows the percent of bipolar and amacrine cells at different eccentricities across the retina. Scale = 50 μm.

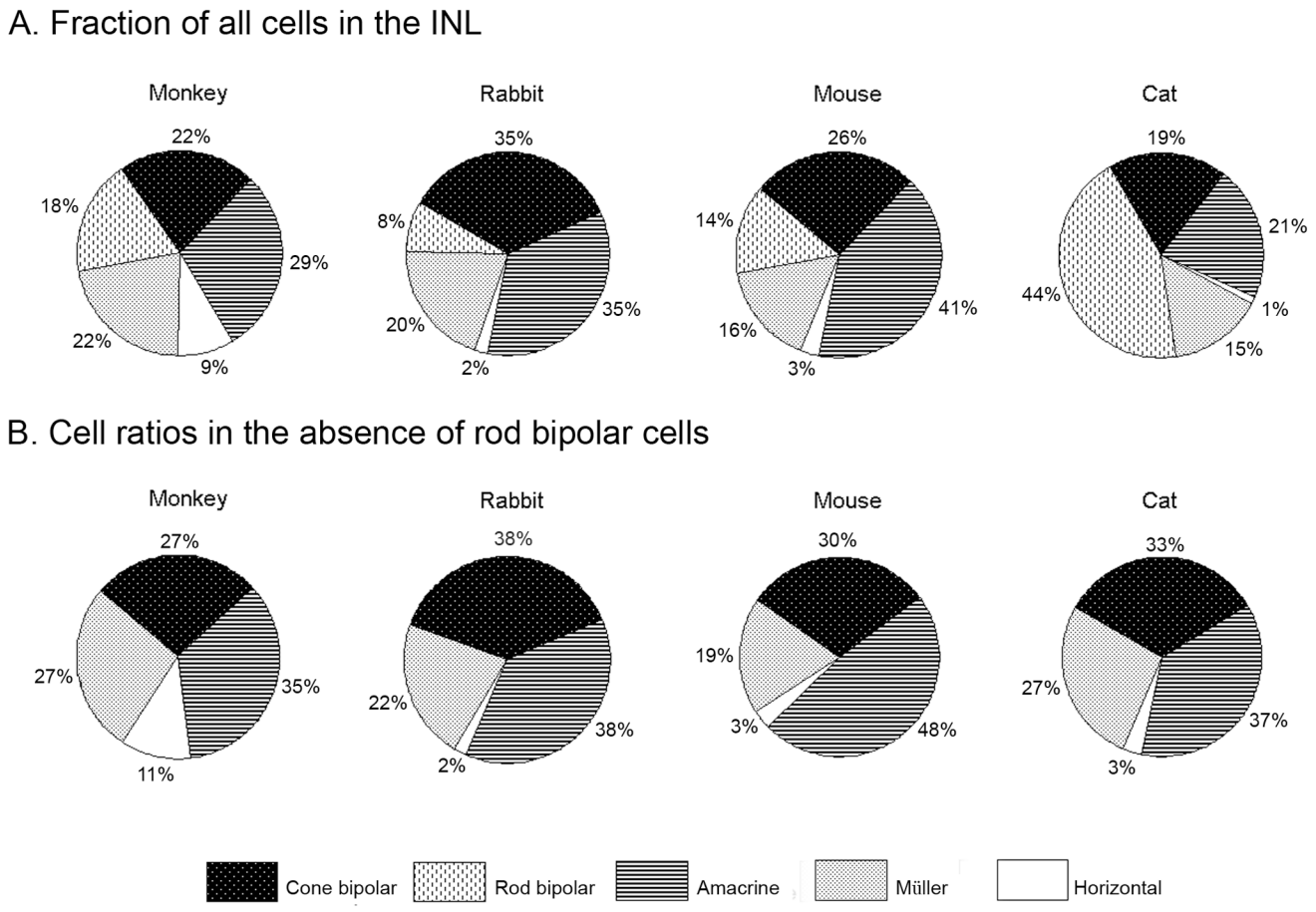

Figure 6.

A. Fractions of bipolar, amacrine, horizontal and Müller cells in monkey, rabbit and cat retinas. B. Ratio of cone bipolar, amacrine, horizontal and Müller cells in monkey, rabbit and cat retinas computed without rod bipolar cells. Data for rabbit, mouse and monkey retinas are from Strettoi and Masland (1995), Jeon et al. (1998) and Strettoi and Volpini (2002).

Table 1

Distribution of cell classes in the INL of cat retina.

	Eccentricity (mm from area centralis)	**8 Dorsal**	**4**	**3**	**2**	**1**	**Area Centralis**	**1**	**2**	**3**	**4**	**6**	**8 Ventral**
Bipolar cells													
Retina 1	Number of cells	158	212	180	218	236	224	231	226	184	175	132	122
	Relative percent	62.7	61.6	63.4	67.1	61.5	60.9	63.6	61.7	60.1	62.3	60.3	60.7
	Density	39500	50476	47368	54500	56190	56000	57750	62778	54118	54688	41250	30500
Retina 2	Number of cells	114	148	157	180	177	228	139	186	178	151	170	133
	Relative percent	59.7	66.1	66.2	67.2	62.5	65.7	55.6	65.5	65.4	62.4	63.2	61.9
	Density	38000	49333	52333	60000	88500	76000	57917	84546	80909	50333	42500	36944
Retina 3	Number of cells	120	147	166	183	195	204	231	170	181	156	143	130
	Relative percent	60	62.6	61	65.1	62.3	62.8	67.2	59.4	61.4	61.4	59.6	62.5
	Density	30000	45938	55333	61000	65000	63750	77000	53125	56563	48750	35750	26000
	Average density	**35833**	**48582**	**51678**	**58500**	**69897**	**65250**	**64222**	**66816**	**63863**	**51257**	**39833**	**31148**
Amacrine cells													
Retina 1	Number of cells	48	71	56	60	91	90	78	81	74	62	48	36
	Relative percent	19	20.6	19.7	18.5	23.7	24.5	21.5	22.1	24.2	22.1	21.9	17.9
	Density)	12000	16905	14737	15000	21667	22500	19500	22500	21765	19375	15000	9000
Retina 2	Number of cells	33	34	44	47	62	82	70	57	49	53	51	40
	Relative percent	17.3	15.2	18.6	17.5	21.9	23.6	28	20.1	18	21.9	19	18.6
	Density	11000	11333	14667	15667	31000	27333	29167	25909	22273	17667	12750	11111
Retina 3	Number of cells	33	46	59	58	69	80	61	70	66	56	48	38
	Relative percent	16.5	19.6	21.7	20.6	22	24.6	17.7	24.5	22.4	22	20	18.3
	Density	8250	14375	19667	19333	23000	25000	20333	21875	20625	17500	12000	7600
	Average density	**10417**	**14204**	**16357**	**16667**	**25222**	**24944**	**23000**	**23428**	**21554**	**18181**	**13250**	**9237**
Horizontal cells													
Retina 1	Number of cells	3	3	5	4	6	4	8	8	5	4	4	3
	Relative percent	1.2	0.9	1.8	1.2	1.6	1.1	2.2	2.2	1.6	1.4	1.8	1.5
	Density	750	714	1316	1000	1429	1000	2000	2222	1471	1250	1250	750
Retina 2	Number of cells	1	2	3	4	5	4	6	5	4	3	1	1
	Relative percent	0.5	0.9	1.3	1.5	1.8	1.2	2.4	1.8	1.5	1.2	0.4	0.5

	Eccentricity (mm from area centralis)	8 Dorsal	4	3	2	1	Area Centralis	1	2	3	4	6	8 Ventral
	Density	333	667	1000	1333	2500	1333	2500	2272.7	1818.2	1000	250	278
Retina 3	Number of cells	3	6	4	2	5	4	2	5	3	3	3	3
	Relative percent	1.5	2.6	1.5	0.7	1.6	1.2	0.6	1.7	1	1.2	1.3	1.4
	Density	750	1875	1333	667	1667	1250	667	1563	938	938	750	600
	Average density	**611**	**1085**	**1216**	**1000**	**1865**	**1194**	**1722**	**2019**	**1409**	**1063**	**750**	**543**
Müller cells													
Retina 1	Number of cells	43	58	43	43	51	50	46	51	43	40	35	40
	Relative percent	17.1	16.9	15.1	13.2	13.3	13.6	12.7	13.9	14.1	14.2	16	19.9
	Density	10750	13810	11316	10750	12143	12500	11500	14167	12647	12500	10938	10000
Retina 2	Number of cells	43	40	33	37	39	33	35	36	41	35	47	41
	Relative percent	22.5	17.9	13.9	13.8	13.8	9.5	14	12.7	15.1	14.5	17.5	19.1
	Density	14333	13333	11000	12333	19500	11000	14583	16364	18636.4	11667	11750	11389
Retina 3	Number of cells	44	36	43	38	44	37	50	41	45	39	46	37
	Relative percent	22	15.3	15.8	13.5	14.1	11.4	14.5	14.3	15.3	15.4	19.2	17.8
	Density	11000	11250	14333	12667	14667	11563	16667	12814	14063	12188	11500	7400
	Average density	**12028**	**12798**	**12216**	**11917**	**15437**	**11688**	**14250**	**14448**	**15115**	**12118**	**11396**	**9596**
Average density INL (cells/mm^2)		**58889**	**76670**	**81468**	**88083**	**112421**	**103076**	**103195**	**106712**	**101942**	**82619**	**65229**	**50524**